Chapter 9

Molecular Simulations on Interfacial Sliding of Carbon Nanotube Reinforced Alumina Composites

Yuan Li, Sen Liu, Ning Hu, Weifeng Yuan and Bin Gu

Additional information is available at the end of the chapter

http://dx.doi.org/10.5772/48816

1. Introduction

With remarkable physical and mechanical properties [1, 2], carbon nanotube (CNT), either single-walled carbon nanotube (SWCNT) or multi-walled carbon nanotube (MWCNT), has prompted great interest in its usage as one of the most promising reinforcements in various matrices (e.g., polymers, metals and ceramics) [3-11]. However, the dramatic improvement in mechanical properties has not been achieved so far. The reason can be attributed to several critical issues: (1) insufficient length and quality of CNT, (2) poor CNT dispersion and alignment, and (3) weak interface between CNT and matrix. Although great progress has been made to improve the first two issues by developing newly cost-effective CNT synthesis methods and exploring specific fabrication methods of composites (e.g., spark plasma sintering [12], sol-gel process [13]), the proper control of interfacial properties is still a challenge as the inherent characteristics is unclear.

Up to date, large amounts of investigations have been focused on the interfacial properties of polymer-based composites by using direct pull-out experiments with the assistance of advanced instruments (e.g., transmission electronic microscopy (TEM) [14,15], atom force microscope (AFM) [16,17], Raman spectroscopy [18], scanning probe microscope (SPM) [19]), or theoretical analysis based on continuum mechanics (e.g., cohesive zone model [20], Cox's model [21], shear lag model [22,23] and pull-out model [24,25]), or atomic simulations [26-33]. However, in contrast, much less work has been focused on the interfacial properties of alumina-based composites [34-38]. For example, it has been reported that there are three hallmarks of toughening behavior demonstrated in CNT-reinforced alumina composites (CNT/Alumina) as below [34]: crack deflection at the CNT/Alumina interface; crack bridging by CNT, and CNT pull-out on the crack plane, which is consistent with that in conventional

INTECH
open science | open minds

© 2012 Li et al., licensee InTech. This is an open access chapter distributed under the terms of the Creative Commons Attribution License (http://creativecommons.org/licenses/by/3.0), which permits unrestricted use, distribution, and reproduction in any medium, provided the original work is properly cited.

micron-scale fiber reinforced composites. Therefore, a fundamental understanding on the interfacial sliding between CNT and alumina matrix (i.e., CNT pull-out from alumina matrix) is important for clarifying the interfacial properties, and therefore the mechanical properties of bulk CNT/Alumina composites.

Current experimental works have reported two common sliding behaviors in CNT/Alumina composites: the pull-out of SWCNT [35] and sword-in-sheath mode [36, 37] of MWCNT (i.e. "pull-out of the broken outer walls of CNT with matrix", or "pull-out of inner walls of CNT with matrix after the breakage of the outer walls" in relativity). Therefore, clarifying the above two distinguished pull-out behaviors is of critical importance for understanding the interfacial properties of CNT-reinforced composites.

In this Chapter, a series of pull-out simulations of either SWCNT or MWCNT from alumina matrix are carried out based on molecular mechanics (MM) to investigate the corresponding interfacial sliding behaviors in CNT/Alumina composites. By systematically evaluating the variation of potential energy increment during the pull-out process, the effects of grain boundary (GB) structures of alumina matrix, nanotube length, nanotube diameter, wall number and capped structure of CNTs are explored for the first time.

2. Computational model

As experimentally identified, CNTs are generally located in the GB of alumina [34-37, 39], which can be schematically illustrated in Fig. 1. Note that the GB structure is generally characterized by a multiplicity index Σ based on the geometrical concept of three-dimensional (3D) coincidence between two crystals named the coincidence site lattice (CSL) model [40], which is defined as the ratio of the crystal lattice sites density to the density of the two grain superimposed lattices.The corresponding computational model by using the commercial software of Materials Studio (Accelrys) can be constructed as follows:

1. Building a hexagonal primitive cell of neutral alumina;
2. Cleaving the required GB planes and joining them together;
3. Inserting a CNT into the GB;
4. Relaxing the constructed model to obtain the equilibrated configuration.

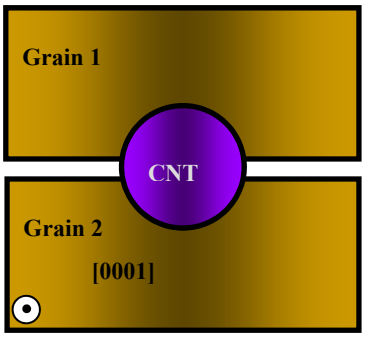

Figure 1. Schematic GB with CNT

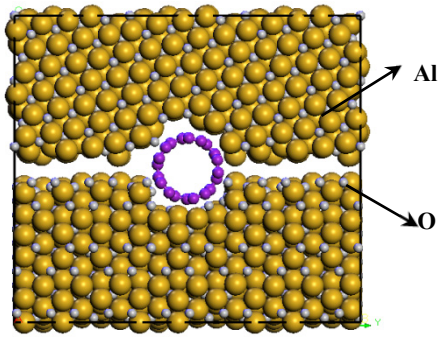

Figure 2. Simulation cell of GB with CNT

As an example, the equilibrated model of Σ7 $(14\bar{5}0)//(41\bar{5}0)$ [41] GB is shown in Fig. 2, in which the inserted open-ended SWCNT (5,5) has the length of l=5.17nm and diameter of D=0.68nm.

The pull-out process of CNT is schematically given in Fig.3, which is mainly divided into the following two steps:

1. Applying the fixed boundary conditions to the left end of alumina matrix;
2. Pulling out the CNT gradually along its axial (x-axis) direction with a constant displacement increment Δx of 0.2nm.

After each pull-out step, the structure should be relaxed in order to obtain the minimum systematic potential energy E.

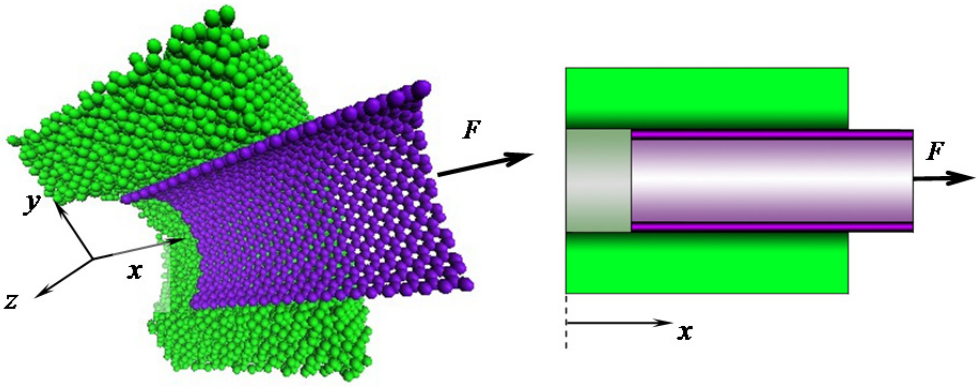

Figure 3. Schematic pull-out process of CNT from alumina matrix
(green balls: atoms in alumina matrix, purple balls: atoms of CNT)

3. Pull-out simulations of open-ended SWCNTs from alumina matrix

3.1. Effect of GB structure

To a large extent, GBs play a significant role on the microstructure formation and properties control of polycrystalline materials. To explore the influence of GB structure on the interfacial siding behavior between CNT and alumina matrix, three representative GB structures with a common rotation axis of [0001] ($\Sigma3(11\bar{2}0)//(11\bar{2}0)$ [42], $\Sigma7(14\bar{5}0)//(41\bar{5}0)$ [41,43,44], and $\Sigma31(47\overline{11}0)$ // $(74\overline{11}0)$ [44]) are modeled. Note that the same fragment of SWCNT(5,5) with the length of l=5.17nm and diameter of D=0.68nm is employed.

The obtained variations of energy increment ΔE between two consecutive pull-out steps are plotted in Fig. 4, where three distinct stages can be clearly seen for each case. In the initial ascent stage *I*, ΔE increases sharply until the pull-out displacement x reaches up to about 1.0nm. After that ΔE undergoes a long platform stage *II* followed by the quick descent stage *III* until the complete pull-out. It is noticeable that both stages *I* and *III* have the same range corresponding to the pull-out displacement of approximately a=1.0nm, which is very close to the cut-off distance of vdW interaction (i.e., 0.95nm). This feature of ΔE is similar to that for the pull-out process of CNT from polymer matrix [33] and that for the sliding among nested walls in a MWCNT [45].

Moreover, ΔE in these three curves are almost identical in stages *I* and *III*, and have the same average value at stage *II* although Σ7 GB results in a slightly higher ΔE. This suggests that the GB structure of alumina matrix has only a limited effect on the energy increment ΔE between two adjacent pull-out steps.

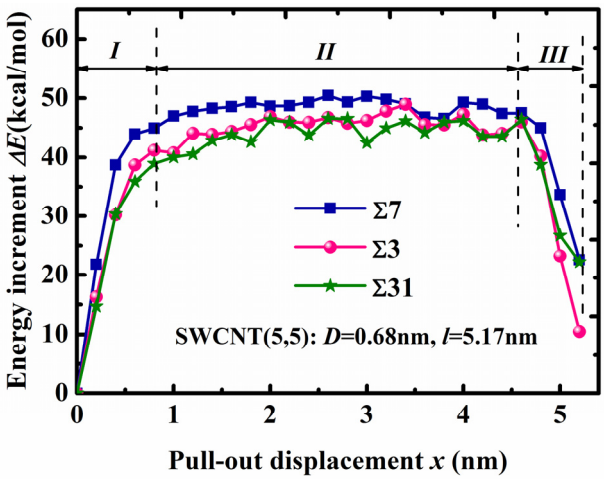

Figure 4. Effect of GB structure on the variation of energy increment during the pull-out process

Here, as discussed in Refs. [33,45], the stable pull-out stage *II* is focused on, in which the average energy increment in stage *II* is referred to as ΔE_{II} hereinafter. Obviously, ΔE_{II} is

independent of GB structure of alumina matrix. Therefore, in the following simulations, the Σ31 GB structure is employed to investigate the effect of nanotube length and diameter on the pull-out process.

3.2. Effect of nanotube length

To investigate the effect of nanotube length on the pull-out process, three SWCNTs (5,5) with different lengths are embedded in the same Σ31 GB of alumina matrix, respectively. The obtained variations of energy increment ΔE between two adjacent pull-out steps are given in Fig.5, in which the same trend is clearly observed for each case as that in Fig. 4. Moreover, the identical ΔE_{II} of three cases indicates its *independence of nanotube length*. Therefore, in the following simulations, CNTs with the same length of 5.17nm are employed.

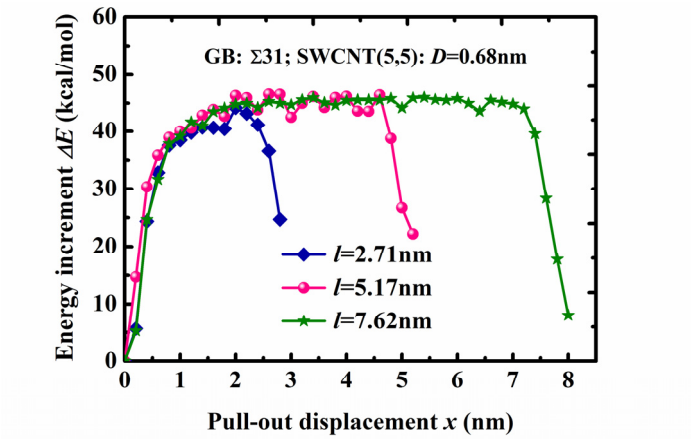

Figure 5. Effect of nanotube length on the variation of energy increment during pull-out process

3.3. Effect of nanotube diameter

Based on the above length-independent behavior, four SWCNTs (i.e., (5,5), (10,10), (15,15), (20,20)) with the same length of 5.17nm but different diameters are embedded into alumina matrix with Σ31GB structure. The corresponding relationship between energy increment ΔE and pull-out displacement x is shown in Fig.6a. Unlike the length-independent behavior, *ΔE_{II} increases linearly with nanotube diameter* as fitted in Fig.6b with the following formula

$$\Delta E_{II} = 52.04 \times D + 9.04 \tag{1}$$

where ΔE_{II} is in kcal/mol, and D is in nm.

This phenomenon can be attributed to the number of atoms in circumferential direction, which increases linearly with nanotube diameter. For a CNT with larger diameter, there will be stronger vdW interactions needed to be overcome for the possible pull-out, which subsequently induces the higher energy increment in the same pull-out displacement.

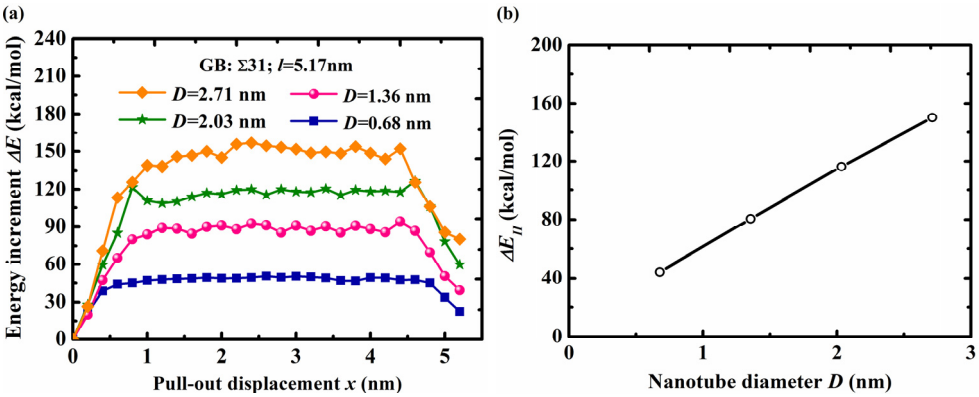

Figure 6. Effect of nanotube diameter on the variation of energy increment during the pull-out process (a) Relationship of energy increment and pull-out displacement; (b) Relationship of ΔE_{II} and nanotube diameter

3.4. Pull-out force and surface energy density

As discussed above, for the pull-out of a SWCNT, the corresponding average energy increment in stage *II*, i.e., ΔE_{II}, is independent of GB structure and nanotube length, but is proportional to nanotube diameter. In view of that the work done by the pull-out force is equal to the energy increment in each pull-out step by neglecting some other minor energy dissipations, the pull-out force can be approximately calculated as

$$F_{II} = \frac{\Delta E_{II}}{\Delta x} \tag{2}$$

On this sense, we can conclude that *the pull-out force of CNT from alumina matrix related to energy increment is also independent of GB orientation and nanotube length, but is proportional to nanotube diameter*. From Eqs. (1) and (2), the corresponding empirical formula to predict the pull-out force is proposed as

$$F_{II} = 1.81 \times D + 0.31 \tag{3}$$

where F_{II} is in the unit of nN, and D of nm.

It should be noted that two new surface regions are generated at two ends of CNT after each pull-out step (i.e., the inner surface of the matrix at the left side of CNT, and the outer surface of CNT on the right side). Therefore, the corresponding surface energy should be equal to the energy increment. Therefore, the surface energy density can be calculated as

$$\gamma_{II} = \frac{\Delta E_{II}}{2\pi D \Delta x} = \frac{F_{II}}{2\pi D} \tag{4}$$

Initially, this value is dependent on the diameter of SWCNT. However, as nanotube diameter increases, it will decrease gradually and then saturate to a constant. The converged

value of surface energy density is approximately 0.3N/m. Note that this surface energy density is newly reported for the interface of SWCNT and alumina matrix, although there have been some reports about that for the interface of SWCNT and polymer matrix with the value of 0.09~0.12N/m [26, 30] or for sliding interface among nested walls in a MWCNT with the value of 0.14N/m [45]. It can be found that the surface interface density in CNT/Alumina composites is much higher than those of CNT/Polymer composites or CNT walls, implying its stronger interface.

3.5. Interfacial shear stress

Based on the above discussion, the corresponding interfacial shear stress is analyzed in the following.

The pull-out force is equilibrated with the axial component of vdW forces which induces the interfacial shear stress. Conventionally, if we employ the common assumption of constant interfacial shear stress with uniform distribution along the whole embedded region of CNT, the pull-out force F_{II} will vary with the embedded length of CNT, which is obviously in contradiction to the above length-independent behavior of average energy increment ΔE_{II} in stage *II*. For the extreme case of a CNT with an infinite length, the interfacial shear stress tends to be zero, which is physically unreasonable. This indicates that the conventional assumption of interfacial shear stress is improper for the perfect interface of CNT/Alumina composites with only consideration of vdW interactions.

For this problem, the interfacial shear stress should be analyzed according to the different stages in the variation of energy increment ΔE. In stage *I*, the interfacial shear stress exists within a region of the length a=1.0nm at each end of CNT as described in Ref. [45] since the length of CNT in the model is equal to that of alumina matrix. In stage *II*, the situation may be different since the left end of CNT is deeply embedded into the alumina matrix with the pull-out displacement x much larger than a=1.0nm. To address the interfacial shear stress in this stage *II*, a simple simulation is performed here.

As shown in Fig. 7a, a SWCNT(5,5) with only a half repeat unit is completely embedded in the middle position of alumina matrix. Then this SWCNT fragment is pulled out gradually with a constant increment of Δx=0.2nm to obtain the variation of systematic energy increment ΔE_{ω}, and the corresponding pull-out force F_{ω}. As this SWCNT fragment is very short, the obtained pull-out force F_{ω}, which is equilibrated by the shear force induced by the interfacial shear stress, can be used to characterize the distribution of interfacial shear stress. The obtained distribution of pull-out force F_{ω} at various pull-out steps is shown in Fig.7b. At the initial stage of the pull-out, the pull-out force keeps value at zero. When the CNT unit cell moves into the range of a=1.0nm measured from the right end of alumina matrix, the pull-out force increases sharply. It reaches the maximum when the CNT unit cell is just located on the right end of the matrix. As the CNT unit cell is further pulled out, it decreases gradually to zero. In virtue of the above results, as shown in Fig. 7c, the interfacial shear stress is solely distributed within the region of 2a centered by the right end of matrix in

stage *II*. The pull-out force during the pull-out process is further averaged within the range of 2*a*, i.e., F_{ω}^{*}=0.09nN in Fig. 7b.

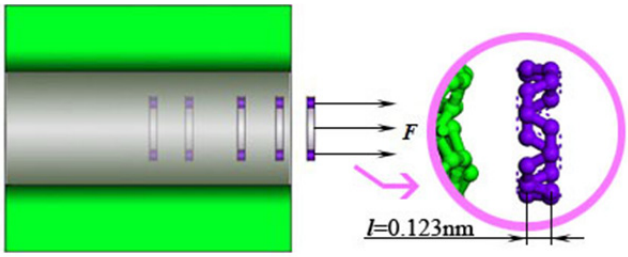

(a) Model for the pull-out of a simple CNT unit cell

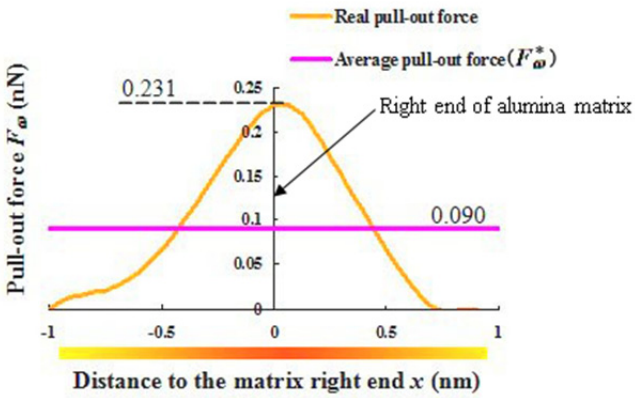

(b) Variation of pull-out force F_{ω} and average pull-out force F_{ω}^{*}

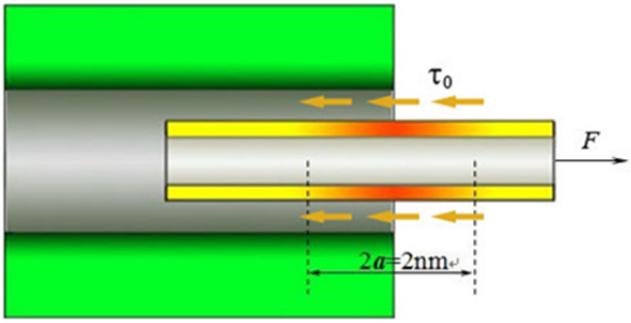

(c) Distribution of average interfacial shear stress

Figure 7. Analysis of interfacial shear stress

By assuming that the interfacial shear stress is uniform within the above defined region for simplicity, the average of interfacial shear stress τ_0 in stage *II* can be defined from the pre-defined average pull-out force(i.e., F_ω^*) as

$$\tau_0 = \frac{F_\omega^*}{2\pi Da} \tag{5}$$

Obviously, τ_0 is dependent on the diameter *D* of SWCNT. However, it tends to be a constant as nanotube diameter increases gradually. The obtained converged interfacial shear stress τ_0 from various unit cells of SWCNT with different diameters is 303 MPa. Note that it only exists within the range of 2*a* centered by the right end of the matrix.

4. Pull-out simulations of open-ended MWCNTs from alumina matrix

Usually, there are two typical sliding behavior for MWCNT-reinforced composites: one is the complete pull-out of MWCNT, while the other is the so-called sword-in-sheath mode, e.g., in which the broken outer walls are pulled out (i.e., sheath) leaving the intact inner walls (i.e., sword) in the matrix. Therefore, based on the above information, two simple typical cases are firstly investigated: Case 1: pull-out of the whole MWCNT (e.g., Fig. 8a); Case 2: pull-out of only the outermost wall of MWCNT (e.g., Fig. 8b).

In view of the extremely high computational cost, several double-walled carbon nanotubes (DWCNTs) with wall number *n*=2 and triple-walled carbon nanotubes (TWCNTs) with wall number *n*=3 are discussed in the present simulation. The obtained average energy increment ΔE_{II} in stage *II* related to the pull-out force is also found to be proportional to the diameter of the outermost wall of MWCNT D_o, which can be fitted as

Case 1

$$\begin{cases} \Delta E_{II} = 57.54 \times D_o + 4.36,\ F_{II} = 2.00 \times D_o + 0.15\ \ (n=2) & \text{(a)} \\ \Delta E_{II} = 58.26 \times D_o + 6.50,\ F_{II} = 2.03 \times D_o + 0.23\ (n=3) & \text{(b)} \end{cases} \tag{6}$$

Case 2

$$\begin{cases} \Delta E_{II} = 93.61 \times D_o + 10.17,\ \ F_{II} = 3.26 \times D_o + 0.35\ \ (n=2) & \text{(a)} \\ \Delta E_{II} = 96.60 \times D_o + 10.50,\ \ F_{II} = 3.33 \times D_o + 0.37\ \ (n=3) & \text{(b)} \end{cases} \tag{7}$$

For Case 1, the relationship of ΔE_{II} and nanotube diameter for the complete pull-out of SWCNT (Eq. 3), DWCNT (Eq. 6a), and TWCNT (Eq.7a) are plotted in Fig. 9, which indicates the effect of wall number from some aspect. The slope for DWCNT is about 9.56% higher than that for SWCNT, which highlights the contribution of the first adjacent inner wall to ΔE_{II}. However, the slope of TWCNT is only about 1.24% higher than that for DWCNT, which implies that the contribution of the second inner wall is gradually weakened as the distance from the sliding interface increases. Therefore, it can be concluded that the pull-out of MWCNT from alumina matrix is mostly affected by its two adjacent walls from the sliding interface, which indicates that for the whole pull-out of any

MWCNT with more walls over 3, ΔE_{II} can be approximately assumed to be equal to that of TWCNT (i.e., Eq. 6b).

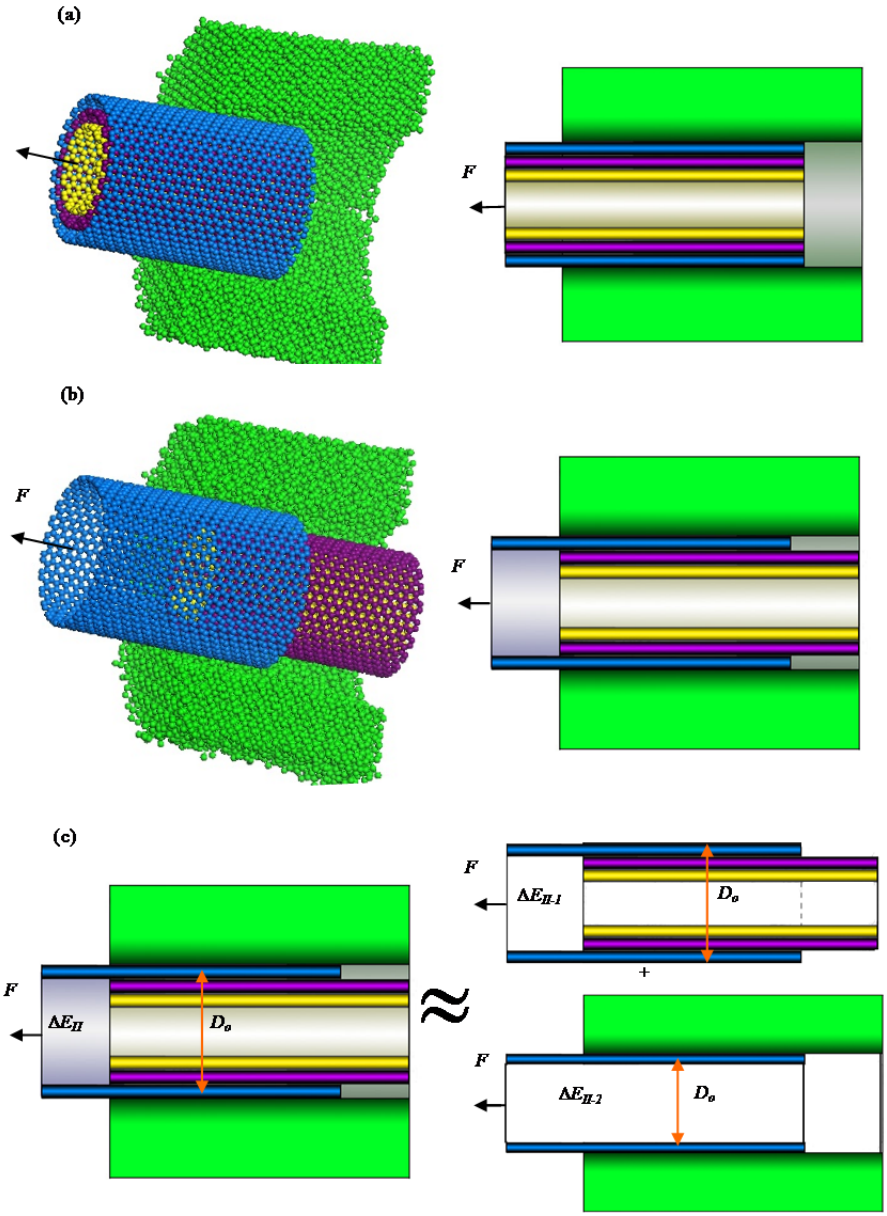

Figure 8. Two typical pull-out cases for an open-ended TWCNT
(a) Case 1: pull-out of the whole MWCNT; (b) Case 2: pull-out of the outmost wall of MWCNT;
c) Decomposition of Case 2 into two independent sub-problems

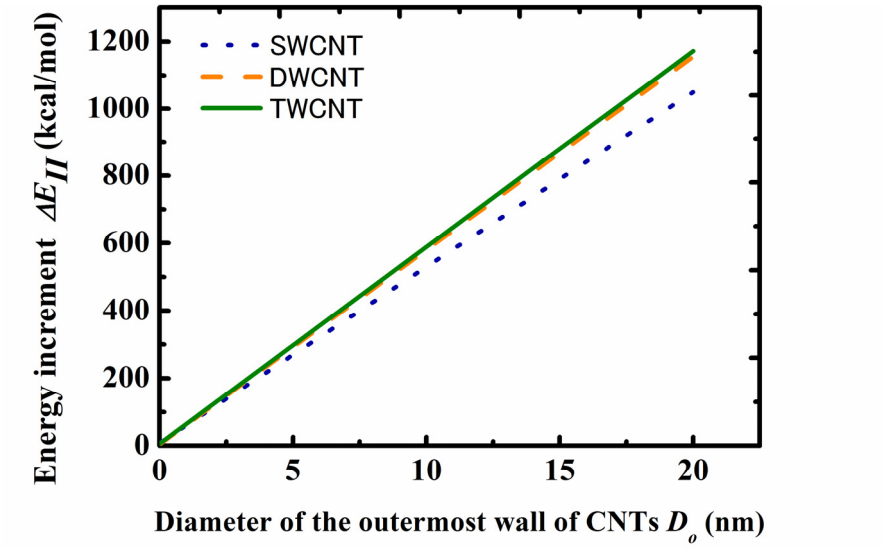

Figure 9. Effect of wall number on the energy increment for the pull-out of whole MWCNT

For Case 2, taking TWCNT(5,5)/(10,10)/(15,15) as an example, it is surprising to find that the corresponding ΔE_{II} is approximately equal to the sum of those of two sub-problems, i.e., the pull-out of a SWCNT(15,15) from alumina matrix, and the pull-out of the outermost wall in the TWCNT. Therefore, the corresponding ΔE_{II} for the pull-out of any TWCNT from alumina matrix (i.e., Eq. 7b) can be approximately decomposed into the following two items as given in Fig. 8c: $\Delta E_{II\text{-}1}$ for the pull-out of the outermost wall of TWCNT against the other two inner walls (i.e., Eq. 5 in Ref. [45]), and $\Delta E_{II\text{-}2}$ for the pull-out of a SWCNT from alumina matrix (i.e., Eq. 3) whose diameter is equal to the outermost wall of the TWCNT.

It should be noted that for the real sword-in-sheath fracture mode, there are more than 3 walls pulled out. For example, as shown in Fig. 10a, several purple outer walls of a MWCNT are pulled out leaving the yellow inner walls within the matrix. Here, there are two sliding interfaces: one is between CNT and matrix, the other is between outer walls and inner wall. According to the above discussion, it can also be thought of as the superimposition of the following two sub-problems in Fig. 10b: one is the pull-out of the TWCNT which is composed of the outer three walls (i.e., Eq. 6b), and the other is the pull-out of outer three walls in a MWCNT with five walls (i.e., Eq. 6 in Ref. [45]). It indicates that the corresponding ΔE_{II} and pull-out force F_{II} can be calculated as

$$\Delta E_{II} = 58.26 \times D_o + 37.56 \times D_c - 4.00 \tag{8}$$

$$F_{II} = 2.04 \times D_o + 1.31 \times D_c - 0.14 \tag{9}$$

Here, D_o is the diameter of the outermost wall of MWCNT, and D_c is the diameter of the green critical wall in Fig. 10 (i.e., the immediate outer wall at the sliding surface between outer walls and inner walls).

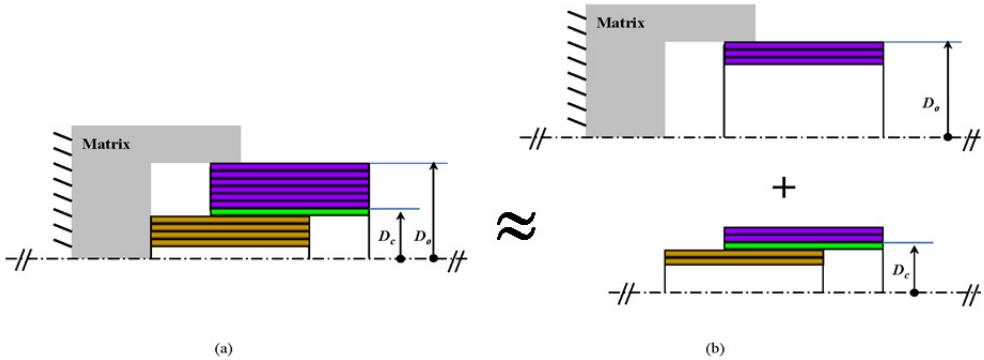

Figure 10. Real case of sword-in-sheath mode

5. Pull-out simulations of a capped MWCNT from alumina matrix

It is noted that open-ended CNTs are employed in the above simulations. On the other hand, it has been reported that CNT cap makes great effect on its field emission properties [46], load transferring ability among nested walls of MWCNT [45, 47, 48]. However, to our best knowledge, there is no any detailed report on the effect of CNT caps on the interfacial properties of CNT-reinforced composites. Therefore, the pull-out of capped MWCNTs from alumina matrix in a sword-in-sheath mode is discussed here.

The schematic model is given in Fig. 11. By using the principal of superimposition, this pull-out process can be decomposed into the following three parts: pull-out of outer walls against matrix (i.e., part I); pull-out of inner walls against outer walls, which can be further decomposed into the open-ended part of inner/outer walls (i.e., part II) and the capped part of inner/outer walls (i.e., part III) as each wall in a MWCNT is composed of open-ended part and capped part.

Generally, the number of broken outer walls and intact inner walls are more than 3. Therefore the corresponding pull-out forces for the above three parts are analyzed as below.

i. Pull-out of outer walls against matrix (i.e., part I in Fig. 11): According to Eq. 2, the corresponding pull-out force F_1 can be predicted by using Eq. 6b, i.e.,

$$F_1 = 2.03 \times D_o + 0.23 \tag{10}$$

ii. Pull-out of open-ended part of inner walls against outer walls (i.e., part II in Fig. 11): According to Eq. 6 in Ref. [45], the corresponding pull-out force F_2 can be predicted as

$$F_2 = 1.31 \times D_c - 0.37 \tag{11}$$

iii. Pull-out of capped part between inner walls and outer walls (i.e., part III in Fig. 11): This part can be transferred as the interfacial sliding among nested walls in a capped MWCNT.

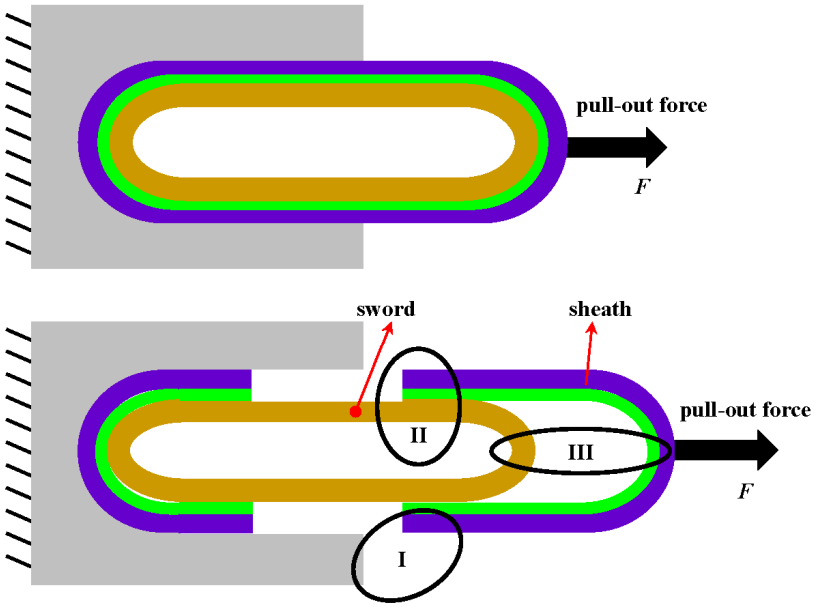

I: outer walls/matrix; II: open-ended part of inner/outer walls; III: capped part of inner/outer walls

Figure 11. Schematic model for the pull-out of a capped MWCNT from alumina matrix

As illustrated in Fig. 12a, after fixing the atoms of the outer cap, the inner wall is pulled out along its axial direction by applying a constant displacement increment of Δx_2=0.01nm on the atoms of the right end of inner wall. Note that the present displacement increment Δx_2 is smaller than the above Δx of 0.2nm, which is used for making the effect of CNT caps on energy increment clearly. After each pull-out step, the structure is relaxed to obtain the minimum potential energy E. As discussed in Ref. [45], the pull-out force of an open-ended CNT is only proportional to nanotube diameter, and independent of nanotube length. For this reason, five DWCNTs with different diameters but same length are built up to investigate the effect of CNT cap. The calculated energy increments between two consecutive pull-out steps of three DWCNTs are shown in Fig. 13a, where D_c is the diameter of critical wall (i.e., the outer wall of DWCNT). It can be seen that for each DWCNT the energy increment ΔE increases rapidly up to a peak value at a specified displacement, and then decreases. The same feature is also observed in the simulations of two other DWCNTs with larger diameters, i.e., (54,54)/(59,59) with D_c=8.0nm and (83,83)/(88,88) with D_c=11.93nm. The maximum energy increment (i.e., ΔE_{max}) for the five DWCNTs is shown in Fig. 13b. The relationship between ΔE_{max} and D_c can be perfectly fitted into a quadratic function of

$$\Delta E_{\max-\mathrm{DWCNT}} = 2.09 \times D_c^2 - 2.15 \times D_c + 0.94 \tag{12}$$

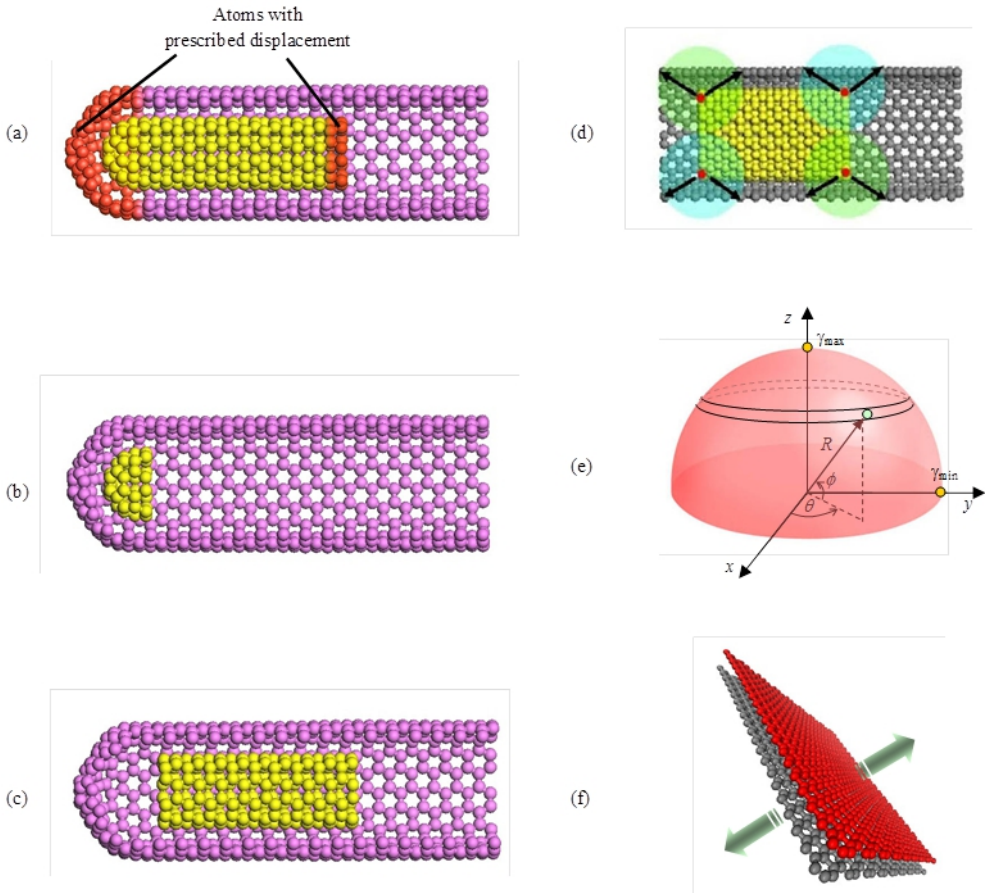

Figure 12. Interfacial sliding in a capped DWCNT
(a) Schematic model of a capped DWCNT; (b) Pull-out of the capped part;
(c) Pull-out of the open-ended part;
(d) Force state of open-ended part of CNT; (e) Estimation of energy variation of a cap;
(f) Pull-out of graphite sheets

To understand this potential energy increment in detail, we further divided the inner wall (Fig. 12a) into two parts, i.e., the capped (Fig. 12b) and the open-ended part (Fig. 12c). The corresponding pull-out forces for these two parts are F_3^1 and F_3^2, which means $F_3 = F_3^1 + F_3^2$. The pull-out of open-ended part (Fig. 12c) does not cause any change of the potential energy, i.e., $F_3^2=0$. It means that the contribution of capped part, i.e., F_3^1 dominates the total pull-out force F_3. The reason can be explained using Fig. 12d-12e.

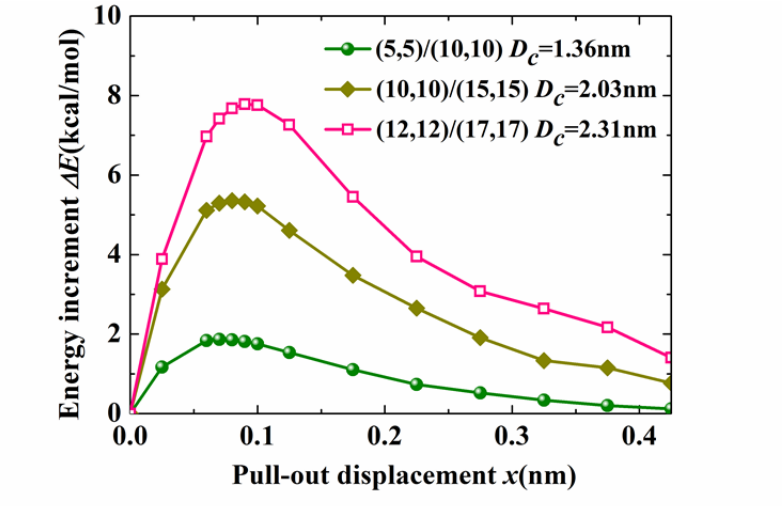

(a) Energy increment versus pull-out displacement for model of Fig.12a

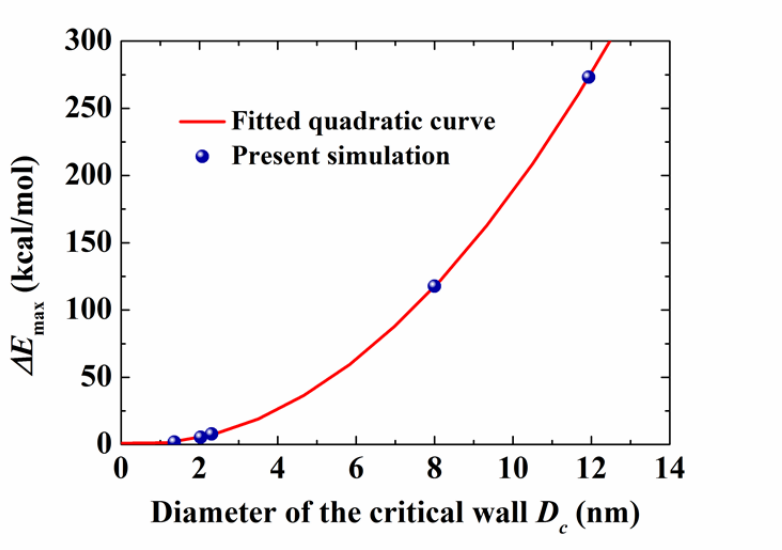

(b) Relationship between maximum energy increment and nanotube diameter

Figure 13. Variation of energy increment for the interfacial sliding in a capped DWCNT

First, in Fig. 12d, if the length of the outer wall of DWCNT is long enough, the carbon atoms of the inner wall are always in force equilibrium. For example, in Fig. 12d, the atoms in red are balanced by the symmetrical horizontal forces form the atoms of the outer wall, which are within the cut-off distance of Lennard-Jones potential [49,50]. During a pull-out process, the relative motion of the atoms between the inner wall and outer wall creates repetitive breaking and reforming of the vdW interactions and no resultant resistance force can be generated on the inner wall, i.e., F_3^2=0.

The quadratic form of the energy increment in Eq. 12 due to the capped effect is associated with the surface energy density. Considering a cap model shown in Fig. 12e, the bottom edge is just located on the boundary between the capped and open-ended part. If we use γ_{max} and γ_{min} to represent the maximum and minimum surface energy density (i.e., potential energy variation per unit area) under a specified separation displacement, γ_{max} is at the top of the cap while γ_{min} appears at the bottom of the cap. Then, the surface energy density is assumed to vary from the top to the bottom of the cap in the function of $\gamma(\phi) = \gamma_{\max}\cos(90^\circ - \phi) = \gamma_{\max}\sin\phi$., which implies that γ_{min}=0. This is reasonable as F_3^2=0. Then the total surface energy variation of the cap can be calculated as

$$U_{\text{cap}} = \int_0^{2\pi}\left(\int_0^{\frac{\pi}{2}}\gamma(\phi)R\cos\phi \times Rd\varphi\right)d\theta = \frac{\pi D_c^2}{4}\gamma_{\max} \tag{13}$$

From Eq. 13, regardless of the function of $\gamma(\phi)$, the surface energy is always proportional to πD_c^2. As a result, the energy increment induced by the pull-out of the cap can be described by a quadratic function of D_c, which is consistent with Fig. 13b and Eq. 12. Approximately, the γ_{max} at the small top flat area of the cap during the pull-out process can be predicted in the same way by simulating the separation of two flat graphite sheets in Fig. 12f. It is confirmed by the displacement-energy increments curves obtained from the simulation of two graphite sheets which is quite similar with those in Fig. 13a. The corresponding $\gamma_{max\text{-}cap}$ is around 0.03N/m under 0.01 nm separation displacement in the normal direction of two graphite sheets. Substituting this value into Eq. 13 leads to the total surface energy change as: $U_{cap} = \frac{\pi D_c^2}{4}\gamma_{\max-\text{cap}} = 2.76D_c^2$, which is approximately equivalent to Eq. 12. Therefore, it indicates the quadratic form of Eq. 12 is appropriate from the other aspect.

After validating the effectiveness of Eq. 12, the corresponding maximum pull-out force can be simply evaluated by equaling the work done by the pull-out force to the $\Delta E_{max\text{-}DWCNT}$ with the formula of

$$F_{3-DWCNT} = 1.45 \times D_c^2 - 1.49D_c + 0.65 \tag{14}$$

It should be noted that the above analysis is for a capped DWCNT. For the case of MWCNT, a simplified model in Fig. 14 is developed, as only the immediate two outer and inner walls from the sliding interface can affect the corresponding pull-out interface [45]. The evaluated

pull-out force is found to be approximately 29% higher than that for DWCNT due to the contribution of the immediate two outer and inner walls, which means

$$F_{3-\mathrm{MWCNT}} = 1.87 \times D_c^2 - 1.92 D_c + 0.84 \tag{15}$$

Therefore, for the pull-out of a capped MWCNT from alumina matrix in a sword-in-sheath mode, the corresponding pull-out force can be assumed to be the sum of those for the above three parts (i.e., Eq. 10 for part I, Eq. 11 for part II, Eq. 15 for part III):

$$F = F_1 + F_2 + F_{3-\mathrm{MWCNT}} = 1.87 \times D_c^2 + 2.03 D_o - 0.61 \times D_c + 0.7 \tag{16}$$

For the pull-out of a MWCNT numbered as sample 14 in Ref. [37] which has the outermost wall with diameter of D_o=94nm and the critical wall at the sliding interface with diameter about D_c=90nm, the calculated pull-out force using Eq. 16 is 15.28μN, which is in the same scale of experimental value of 19.7 μN [37].

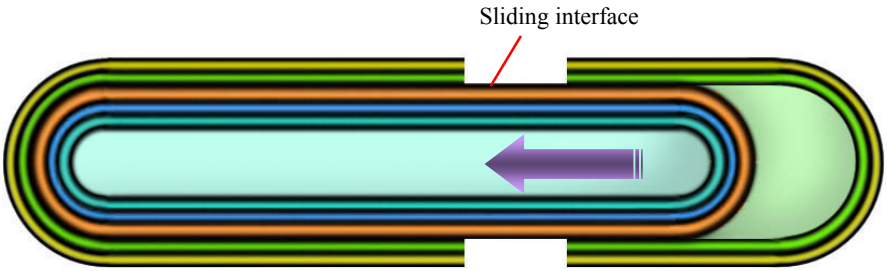

Figure 14. Schematic model for interfacial sliding in a capped MWCNT in sword-in-sheath mode

6. Conclusions

We systematically investigate the pull-out process of open-ended and capped CNTs from alumina matrix using MM simulations, aiming at clarifying the interfacial sliding behavior in CNT/Alumina composites. The effects of grain boundary structure of alumina matrix, nanotube length, nanotube diameter, wall number and capped structure of CNTs are explored systematically.

A set of universal formulae with the newly obtained surface energy density is proposed to approximately predict the pull-out force from nanotube diameter. The philosophy behind these simple empirical formulae is that the pull-out force is only proportional to nanotube

diameter, and independent of nanotube length and GB structure of alumina matrix. The detailed interfacial shear stress is studied in this work, which indicates that the conventional definition of the interfacial shear strength is inappropriate in CNT/Alumina composites. Moreover, there are at most two adjacent walls at each side of the sliding interface which will affect this interfacial sliding in CNT/Alumina composites. Furthermore, it also indicates that CNT caps play a very important role in the pull-out process. These findings will be helpful for clarifying the toughening mechanism for mechanical properties of bulk CNT/Alumina composites and providing useful insight into the design of ideal materials.

Author details

Yuan Li
Department of Nanomechanics, Tohoku University, Aramaki-Aza-Aoba, Aoba-ku, Sendai, Japan

Sen Liu
Department of Mechanical Engineering, Chiba University, Yayoi-cho, Inage-ku, Chiba, Japan

Ning Hu
Corresponding Author
Department of Mechanical Engineering, Chiba University, Yayoi-cho, Inage-ku, Chiba, Japan

Weifeng Yuan and Bin Gu
School of Manufacturing Science and Engineering, Southwest University of Science and Technology, Mianyang, P.R.China

Acknowledgement

The authors are grateful to be partly supported by Tohoku Leading Women's Jump Up Project for 2013 (J1 10002158) and Grand-in-Aids for Scientific Research (No. 19360045 and No. 22360044) from the Ministry of Education, Culture, Sports, Science and Technology (MEXT) of Japan. The authors acknowledge Prof. C.B. Fan (Beijing Institute of Technology, China) for kindly providing the computational resources.

7. References

[1] Dresselhaus MS, Dresselhaus G, Avouris P. (2001) Carbon Nanotubes: Synthesis, Structure, Properties, and Applications. Springer-Verlag Berlin Heidelberg.

[2] Dresselhaus MS, Dresselhaus G, Charlier JC, Hernandez E. (2004) Electronic, Thermal and Mechanical Properties of Carbon Nanotubes. Philosophical Transactions of the Royal Society A. 362:2065-2098.

[3] Thostenson ET, Ren ZF, Chou TW (2001) Advances in the Science and Technology of Carbon Nanotubes and their Composites: A Review. Composites Science and Technology. 61(13): 1899-1912.

[4] Breuer O, Sundararaj U. (2004). Big Returns from Small Fibers: A Review of polymer/carbon nanotube composites. Polymer Composites. 25(6): 630-645.

[5] Coleman JN, Khan U, Blau WJ, Gunko YK. (2006) Small but Strong: A Review of the Mechanical Properties of Carbon Nanotube-Polymer Composites. Carbon. 44:1624-1652.

[6] Moniruzzaman M, Winey KI. (2006) Polymer Nanocomposites Containing Carbon Nanotubes. Macromolecules. 39(16): 5194-5205.

[7] Coleman JN, Khan U, Gun'ko YK. (2006) Mechanical Reinforcement of Polymers Using Carbon Nanotubes. Advanced Materials. 18(6): 689-706.

[8] Peigney A, Laurent C, Flahaut E, et al. (2000) Carbon Nanotubes in Novel Ceramic Matrix Nanocomposites. Ceramics International. 26(6): 677-683.

[9] Curtin WA, Sheldon BW. (2004) CNT-reinforced Ceramics and Metals. Materials Today. 7(11):44-49.

[10] Samal SS, Bal S. (2008) Carbon Nanotube Reinforced Ceramic Matrix Composites- a Review. Journal of Minerals & Materials Characterization & Engineering. 7(4): 355-370.

[11] Cho J, Boccaccini AR, Shaffer M. (2009) Ceramic Matrix Composites Containing Carbon Nanotubes. Journal of Materials Science. 44(8): 1934-1951.

[12] Zhan GD, Kuntz JD, Wan J, Mukherjee Ak. (2003) Single-wall Carbon Nanotube as Attractive Toughening Agents in Alumina-based Nanocomposites. Nature Materials. 2:38-42.

[13] Chan BM, Cha SI, Kim KT, Lee KH & Hong SH. (2005) Fabrication of Carbon Nanotube Reinforced Alumina Matrix Nanocomposite by Sol–gel Process. Materials Science and Engineering A. 395: 124–128.

[14] Qian D, Dickey EC, Andrews R, Rantell T. (2000) Load Transfer and Deformation Mechanisms in Carbon Nanotube-Polystyrene Composites. Applied Physics Letters. 76(20):2868-2870.

[15] Deng F. (2008) Investigation of the Interfacial Bonding and Deformation Mechanism of the Nano Composites Containing Carbon Nanotubes. Tokyo University, PhD Dissertation.

[16] Barber AH, Cohen SR, Kenig S, Wagner HD. (2003) Measurement of Carbon Nanotube-Polymer Interfacial Strength. Applied Physics Letters. 82(23): 4140-4142.

[17] Barber AH, Cohen SR, Kenig S, Wagner HD. (2004) Interfacial Fracture Energy Measurements for Multi-walled Carbon Nanotubes Pulled from a Polymer Matrix. Composite Science and Technology. 64:2283-2289.

[18] Schadler LS, Giannaris SC, Ajayan PM. (1998) Load Transfer in Carbon Nanotube Epoxy Composites. Applied Physics Letters. 73(26):3842-3844.

[19] Cooper CA, Cohen SR, Barber AH, Wagner HD. (2002) Detachment of Nanotubes from a Polymer Matrix. Applied Physics Letters. 81(20):3873-3875.
[20] Jiang LY, Huang Y, Jiang H, Ravichandran G, Gao H, Hwang KC, et al. (2006) A Cohesive Law for Carbon Nanotube/Polymer Interfaces based on the van der Waals Force. Journal of the Mechanics and Physics of Solids. 54: 2436- 2452.
[21] Xiao KQ, Zhang LC. (2004) The Stress Transfer Efficiency of a Single-walled Carbon Nanotube in Epoxy Matrix. Journal of Materials Science. 39:4481-4486.
[22] Gao XL, Li K. (2005) A Shear-lag Model for Carbon Nanotube-Reinforced Polymer Composites. International Journal of Solids and Structures. 42: 1649-1667.
[23] Tsai J, Lu T. (2009) Investigating the Load Transfer Efficiency in Carbon Nanotubes Reinforced Nanocomposites. Composite Structures. 90:172-179.
[24] Lau K. (2003) Interfacial Bonding Characteristics of Nanotube/Polymer Composites. Chemical Physics Letters. 370:399-405.
[25] Natsuki T, Wang F, Ni QQ, Endo M. (2007) Interfacial Stress Transfer of Fiber Pullout for Carbon Nanotubes with a Composite Coating. Journal of Materials Science. 42:4191-4196.
[26] Lordi V, Yao N. (2000) Molecular Mechanics of Binding in Carbon-Nanotube-Polymer Composites. Journal of Materials Research. 15(12):2770-2779.
[27] Liao K, Li S. (2001) Interfacial Characteristics of a Carbon Nanotube-Polystyrene Composite System. Applied Physics Letters. 79(25):4225-4227.
[28] Frankland SJV, Caglar A, Brenner DW, Griebel M. (2002) Molecular Simulation of the Influence of Chemical Cross-links on the Shear Strength of Carbon Nanotube- Polymer Interfaces. Journal of Physical Chemistry B. 106:3046-3048.
[29] Gou J, Minaie B, Wang B, Liang Z, Zhang C. (2004) Computational and Experimental Study of Interfacial Bonding of Single-walled Nanotube Reinforced Composites. Computational Materials Science. 31:225-236.
[30] Zheng Q, Xia D, Xue Q, Yan K, Gao X, Li Q. (2009) Computational Analysis of Effect of Modification on the Interfacial Characteristics of a Carbon Nanotube- Polyethylene Composites System. Applied Surface Science. 255: 3524-3543.
[31] Al-Ostaz A, Pal G, Mantena PR, Cheng A. (2008) Molecular Dynamics Simulation of SWCNT-Polymer Nanocomposite and its Constituents. Journal of Materials Science. 43:164-173.
[32] Chowdhury SC, Okabe T. (2007) Computer Simulation of Carbon Nanotube Pull-out from Polymer by the Molecular Dynamics Method. Composites Part A. 38:747-754.
[33] Li Y, Liu Y, Peng X, Yan C, Liu S, Hu N. (2011) Pull-out Simulations on Interfacial Properties of Carbon Nanotube-reinforced Polymer Nanocomposites. Computational Material Science. 50: 1854-1860.
[34] Xia Z, Riester L, Curtin WA, et al. (2004) Direct Observation of Toughening Mechanisms in Carbon Nanotube Ceramic Matrix Composites. Acta Materialia. 52(4):931-944.

[35] Fan, JP, Zhuang DM, Zhao DQ, et al. (2006) Toughening and Reinforcing Alumina Matrix Composite with Single-wall Carbon Nanotubes. Applied Physics Letters B. 89:121910(3).

[36] Yamamoto G, Omori M, Hashida T, Kimura H. (2008) A Novel Structure for Carbon Nanotube Reinforced Alumina Composites with Improved Mechanical Properties. Nanotechnology. 19:315708(7).

[37] Yamamoto G, Shirasu K, Hashida T, et al. (2011) Nanotube Fracture during the Failure of Carbon Nanotube/Alumina Composites. Carbon. 49: 3709-3716.

[38] Li L, Xia Z, Curtin W, Yang Y. (2009) Molecular Dynamics Simulations of Interfacial Sliding in Carbon-Nanotube/Diamond Nanocomposites. Journal of the American Ceramic Society. 92(10): 2331-2336.

[39] Vasiliev AL, Poyato R, and Padture NP. (2007) Single-wall Carbon Nanotubes at Ceramic Grain Boundaries", Scripta Materialia. 56(6): 461-463.

[40] Bollmann W. (1970) Crystal Defects and Crystalline Interfaces. Springer, Berlin.

[41] Matsunaga K, Nishimura H, Hanyu S, et al. (2005) HRTEM Study on Grain Boundary Atomic Structures Related to the Sliding Behavior in Alumina Bicrystals. Applied Surface Science. 241: 75-79.

[42] Ikuhara Y. (2001) Grain Boundary and Interface Structure in Ceramics. Journal of the Ceramic Society of Japan. 109(7): S110-S120.

[43] Nishimura H, Matsunaga K, Saito T, et al. (2003) Atomic Structures and Energies of Σ7 Symmetrical Tilt Grain Boundaries in Alumina Bicrystals. Journal of the American Ceramic Society. 86(4): 574-580.

[44] Nishimura H, Matsunaga K, Saito T, et al. (2003) Grain Boundary Structures and High Temperature Deformations in Alumina Bicrystals. Journal of the Ceramic Society of Japan. 111(9): 688-691.

[45] Li Y, Hu N, Yamamoto G, Wang Z, et al. (2010) Molecular Mechanics Simulation of the Sliding Behavior between Nested Walls in a Multi-walled Carbon Nanotube. Carbon. 48:2934-2940.

[46] Wang MS, Wang JY, Peng LM. (2006) Engineering the Cap Structure of Individual Carbon Nanotubes and Corresponding Electron Field Emission Characteristics. Applied Physics Letters. 88(24): 243108(1-3).

[47] Shen GA, Namilae S, Chandra N. (2006) Load Transfer Issues in the Tensile and Compressive Behavior of Multi-walled Carbon Nanotubes. Materials Science and Engineering A. 429(1-2):66-73.

[48] Xia Z, Curtin WA. (2004) Pullout Forces and Friction in Multiwall Carbon Nanotubes. Physical Review B. 69:2333408(1-4).

[49] Hu N, Fukunaga H, Lu C, Kameyama M, Yan B. (2005) Prediction of Elastic Properties of Carbon Nanotube Reinforced Composites. Proceedings of the Royal Society A. 461:1685-1710.

[50] Hu N, Nunoya K, Pan D, Okabe T, Fukunaga H. (2007) Prediction of Buckling Characteristics of Carbon Nanotubes. International Journal of Solids and Structures. 44:6565-6550.